Peer-reviewed version available at Entropy 2018, 20, 175; doi:10.3390/e20030175

Type of the Paper (Article)

Quantifying Chaos by Various Computational Methods. Part 1: Simple Systems

J. Awrejcewicz[1*], A.V. Krysko[2], N.P. Erofeev[3], V. Dobriyan[4], M.A. Barulina[5], V.A. Krysko[6]

[1] Lodz University of Technology, Department of Automation, Biomechanics and Mechatronics, 1/15 Stefanowski St., 90-924 Lodz, POLAND; jan.awrejcewicz@p.lodz.pl
[2] National Research Tomsk Polytechnic University, Cybernetic Institute, 30 Lenin Avenue, 634050 Tomsk and Saratov State Technical University, Department of Applied Mathematics and Systems Analysis, 77 Politechnicheskaya Str.,410054 Saratov, RUSSIAN FEDERATION; anton.krysko@gmail.com
[3] Saratov State Technical University, Department of Mathematics and Modeling, 77 Politechnicheskaya Str., 410054 Saratov, RUSSIAN FEDERATION; erofeevnp@mail.ru
[4] Saratov State Technical University, Department of Mathematics and Modeling, 77 Politechnicheskaya Str., 410054 Saratov, RUSSIAN FEDERATION; dobriy88@yandex.ru
[5] Russian Academy of Science, Precision Mechanics and Control Institute, 24 Rabochaya Str., 410028, Saratov, RUSSIAN FEDERATION; marina@barulina.ru
[6] Saratov State Technical University, Department of Applied Mathematics and Systems Analysis, 77 Politechnicheskaya Str., 410054 Saratov, RUSSIAN FEDERATION; tak@san.ru

Abstract: The first part of the paper was aimed at analyzing the given nonlinear problem by different methods of computation of the Lyapunov exponents (Wolf method [1], Rosenstein method [2], Kantz method [3], method based on the modification of a neural network [4, 5], and the synchronization method [6, 7]) for the classical problems governed by difference and differential equations (Hénon map [8], hyper-chaotic Hénon map [9], logistic map [10], Rössler attractor [11], Lorenz attractor [12]) and with the use of both Fourier spectra and Gauss wavelets [13]. It was shown that a modification of the neural network method [4, 5] makes it possible to compute a spectrum of Lyapunov exponents, and then to detect a transition of the system regular dynamics into chaos, hyper-chaos, hyper hyper-chaos and deep chaos [14-16]. Different algorithms for computation of Lyapunov exponents were validated by comparison with the known dynamical systems spectra of the Lyapunov exponents. The carried out analysis helps comparatively estimate the employed methods in order to choose the most suitable/optimal one to study different kinds of dynamical systems and different classes of problems in both this and the next paper parts.

Keywords: Lyapunov exponents, Wolf method, Rosenstein method, Kantz method, neural network method, method of synchronization, Benettin method, Fourier spectrum, Gauss wavelets.

1. Introduction

The first part of the present work was focused on the numerical investigation of classical dynamical systems to estimate velocity of divergence of the neighborhood trajectories with the help of a measure coupled with the Kolmogorov entropy [17] (or metrics). In reference [17], based on the mathematical results of Oseledec [18] and Pesin [19], it was shown that the numerically imposed relations can be treated as exact/true values. The method proposed by Wolf [1] is most widely used to verify and study chaotic dynamics. However, also the Rosenstein [2] and Kantz [3] methods are often employed to estimate the largest Lyapunov exponents. The state-of-the-art of papers devoted to the theoretical background of the Lyapunov exponents and methods of their computations was carried out by Golovko [20]. In particular, the method of the choice of an embedding dimension was described. The method of the correlating dimension, the false nearest neighbor method and the method of gamma-test were presented based on the Hénon and Lorenz attractors. In particular, the occurrence of high computational difficulties was observed in the case of using the Wolf method and its marginally successful employment to small values of the studied data.

To avoid the above-mentioned drawbacks, a novel neural network-based algorithm to estimate the largest Lyapunov exponents by considering only one coordinate has been proposed. Golovko [20] reported the neural network algorithm for computation of a full spectrum of Lyapunov exponents. A comparison of the results obtained by Golovko with the exact values of the Lyapunov exponents of the Lorenz and Hénon systems exhibited small errors.

In references [6, 7], the method of largest Lyapunov computation using the synchronization phenomena of identical systems has been proposed. A few types of coupling have been studied, depending on the type of the considered system. It has been pointed out that large computational time is required to achieve full synchronization.

The method proposed in references [4, 5] is particularly suitable to study chaotic dynamics of continuous mechanical systems. It should be emphasized that, owing to the research results published by the authors of the present paper, the analysis of nonlinear dynamics based on the estimation of the Lyapunov exponents yields a conclusion that the mentioned problems have not been satisfactorily solved yet [1-5].

More recently, Vallejo and Sanjuan [21, 22] have studied the predictability of orbits in coupled systems by means of finite-time Lyapunov exponents. This approach allowed them to estimate how close the computed chaotic orbits were to the real/true orbits, being characterized by the systems shadowing properties.

In the present paper, classical systems (Hénon map [8], hyper-chaotic Hénon map [9], logistic map [10], Rössler attractor [11], and Lorenz attractor [12]) were analyzed with Gauss wavelets, Fourier spectra and Poincaré pseudo-maps.

It is known that the fundamental property of chaos is the existence of strong sensitivity to a change of the initial conditions. The definition of chaos given first by Devaney in 1989 [23] includes three fundamental parts. In addition to sensitivity to the variation of the initial conditions, a condition of mixing, known also as the transitivity condition and the regularity condition, measured by the density of the periodic points or classical notion of periodicity is also included. In 1992, Banks et al. [24] proved that the condition of sensitivity to the initial condition can be neglected, i.e. conditions of transitivity and periodicity imply sensitivity condition.

Knudsen [25] defined chaos as a function given on a bounded metric space which has a dense orbit and essentially depends on initial conditions.

Owing to chaos definition proposed by Gulick [26], chaos exists when either there is essential dependence on the initial conditions or a chaotic function has positive Lyapunov exponents in each point of the space, and which finally does not tend to a periodic orbit. This definition is also employed in the present work.

2. Lyapunov Exponents

2.1. The largest Lyapunov exponent

The following dynamical system was considered

$$\dot{\boldsymbol{x}} = \boldsymbol{f}(\boldsymbol{x}), \tag{1}$$

where x stands for the N-dimensional state vector.

Two closed phase points x_1 and x_2 were chosen (in the phase space). They stand for the origins of the trajectories ($x_1(t)$ and $x_2(t)$). The change in the distance d between two corresponding points of these trajectories under evolution of system (1) can be monitored by:

$$d(t) = |\vec{\varepsilon}(t)| = |x_2(t) - x_1(t)|. \tag{2}$$

If the dynamics of system (1) is chaotic, $d(t)$ increases exponentially in time, i.e.

$$d(t) \approx d(0)e^{kt}. \tag{3}$$

This yields the average velocity of the exponential divergence of the trajectories

$$k \approx \frac{ln\left[\frac{d(t)}{d(0)}\right]}{t}, \tag{4}$$

or more precisely,

$$k = \lim_{\substack{d(0)\to 0 \\ t\to\infty}} \frac{ln[d(t)/d(0)]}{t}. \quad (5)$$

Quantity h is known as the Kolmogorov-Sinai entropy (KS-entropy). Employing the KS-entropy, one can define the studied process, i.e. quantify if the process is regular or chaotic. In particular, if the system dynamics is periodic or quasi-periodic, the distance $d(t)$ is not inversed in time and the KS-entropy is equal to zero ($h = 0$). If the system dynamics tends to a stable fixed point $d(t) \to 0$, then $h < 0$. Contrarily, KS-entropy is positive ($h > 0$) if one deals with chaotic dynamics.

KS-entropy is the maximum characteristic Lyapunov exponent that enables one to follow velocity of information lost with respect to the initial system state.

2.2. Results

The spectrum of Lyapunov exponents makes it possible to qualitatively quantify a local property with respect to stability of an attractor. Consider a phase trajectory $x(t)$ of the dynamical system (1), starting from the point $x(0)$, as well as its neighborhood trajectory $x_1(t)$ as follows

$$x_1(t) = x(t) + \vec{\varepsilon}(t). \quad (6)$$

The following function can be constructed

$$\lambda[\vec{\varepsilon}(0)] = \lim_{t\to\infty} \frac{\ln\left[\frac{|\vec{\varepsilon}(t)|}{|\vec{\varepsilon}(0)|}\right]}{t}, \quad (7)$$

which is defined on the vectors of initial displacement $\vec{\varepsilon}(0)$ such that $|\vec{\varepsilon}(0)| = \varepsilon$, where $\varepsilon \to 0$.

All possible rotations of the initial displacements vector with respect to n directions of the N-dimensional phase space of the function (7) will suffer the jump-like changes in the finite series of the values $\lambda_1, \lambda_2, \lambda_3, ..., \lambda_n$. These values of the function λ are called Lyapunov exponents (LEs). Positive/negative values of LEs can be viewed as a measure of the averaged exponential divergence/convergence of the neighborhood trajectories.

A sum of LEs stands for an averaged divergence of the phase trajectories flow. In the case of a dissipative system, i.e. a system possessing an attractor, this sum is always negative. As numerical case studies show, in some dissipative systems, the LEs are invariant with respect to all chosen initial conditions. This is why a spectrum of LEs can be understood as the property of an attractor.

Usually, LEs are presented in a sequence of LE values in decreasing order. For instance, symbols (+, 0, –) mean that for the analyzed attractor, there is one direction in a 3D space, where exponential stretching is exhibited, the second direction indicates neutral stability, and the third one - exponential compression. It should be noted that all attractors different from stable stationary points always have at least one LE equal to zero (in average sense, all points of a trajectory are bounded by a compact manifold and they cannot exhibit divergence or converge).

In what follows, relationships between the Lyapunov exponents and the properties and types of attractors are illustrated and discussed.

1) $n = 1$. In this case only a stable fixed point can be an attractor (node or focus). There exists one negative LE denoted by $\lambda_1 = (-)$,

2) $n = 2$. In 2D systems, there are two types of attractors: stable nonmovable points and limit cycles. The corresponding LEs follow:

$(\lambda_1, \lambda_2) = (-, -)$ – stable nonmovable/fixed point;

$(\lambda_1, \lambda_2) = (0, -)$ – stable limit cycle (one exponent is equal to zero).

3) $n = 3$. In 3D phase space, there exist four types of attractors: stable points, limit cycles, 2D tori and strange attractors. The following set of LEs characterizes possible dynamical situations to be met:

$(\lambda_1, \lambda_2, \lambda_3) = (-, -, -)$ – stable nonmovable point;

$(\lambda_1, \lambda_2, \lambda_3) = (0, -, -)$ – stable limit cycle;

$(\lambda_1, \lambda_2, \lambda_3) = (0, 0, -)$ – stable 2D tori;

$(\lambda_1, \lambda_2, \lambda_3) = (+, 0, -)$ – strange attractor.

In the majority of studied problems, analytical definition of LEs is not possible, since the analytical solution to the governing differential equations must be known. However, there exist reliable algorithms to find all Lyapunov exponents numerically.

3. Methods of analysis of Lyapunov exponents

3.1. Benettin method [17]

We began with numerical investigation of the Kolmogorov entropy of the Hénon-Heiles model. Numerical computations were carried out with accuracy up to 14 digits by means employing the so-called method of central points. Observe that, independently of the results reported in reference [27], a similar method was used in reference [28].

Based on the Lyapunov exponents, the ergodic properties of dissipative dynamical systems with a few degrees of freedom were numerically studied employing the Lorenz system. The system exhibited the exponents spectrum of the (+, 0, –) type, and the exponents had the same values for the orbits beginning from an arbitrary point on the attractor. It means that the ergodic property of a general dynamical system can be quantified by a spectrum of the characteristic Lyapunov exponents. Below, a brief description of the used method was presented.

Let a point x_0 belong to the attractor A of a dynamical system. An evolution trajectory of the point x_0 is referred to as a real/true trajectory. A positive quantity ε, being significantly less than the attractor dimension, is chosen. Furthermore, an arbitrary perturbed point $\tilde{x}_0$ is chosen in a way to satisfy $\|\tilde{x}_0 - x_0\| = \varepsilon$. The evolution of points x_0 and $\tilde{x}_0$ is considered in a short time interval T, and new points are denoted by x_1 and $\tilde{x}_1$, respectively. A vector $\Delta x_1 = \tilde{x}_1 - x_1$ is called the perturbation vector. The first estimate of the exponent is found with the use of the following formula

$$\tilde{\lambda}_1 = \frac{1}{T} \ln \frac{\| \Delta x_1 \|}{\varepsilon}. \tag{8}$$

The time interval T is chosen in a way to keep the amplitude of perturbation less than the linear dimensions of the phase space nonhomogenity and the attractor dimension. The normalized perturbation vector $\Delta x_1' = \varepsilon \Delta x_1 / \| \Delta x_1 \|$ is taken, and a new perturbed point $\tilde{x}_1 = x_1 + \Delta x_1'$ is defined. Finally, the so far described procedure is implemented taking into account x_1 and $\tilde{x}_1$ instead of x_0 and $\tilde{x}_0$, respectively.

Repeating this procedure M times, λ is defined as an arithmetic average of the estimates $\tilde{\lambda}_1$ obtained on each computational step:

$$\lambda \cong \frac{1}{M} \sum_{i=1}^{M} \tilde{\lambda}_1 = \frac{1}{M} \sum_{i=1}^{M} \frac{1}{T} \ln \frac{\| \Delta x_i \|}{\varepsilon} = \frac{1}{MT} \sum_{i=1}^{M} \ln \frac{\| \Delta x_i \|}{\varepsilon}. \tag{9}$$

In order to achieve a higher estimate, one can take large M and carry out computations for a different initial point x_0. This method can be used when the equations governing the system evolution are known. It should be noted, however, that these equations are usually unknown for the experimental data.

To compute the Lyapunov spectrum numerically, one can use another approach generalizing the Benettin's algorithm. In general, it is necessary to follow a few trajectories of the perturbed points instead of only one, fundamental trajectory (the number of perturbed trajectories is equal to the dimension of the phase space). For this purpose, a numerical approach based on derivation of the dynamic equations in variations can be used [17]. Since the largest LE plays a crucial role in the evolution of all perturbed trajectories, it is necessary to carry out orthogonalization of the perturbation vectors on each step of the algorithm. In what follows, a procedure of numerical estimation of the Lyapunov spectrum of a dynamical system is briefly described. To simplify, the considerations are limited to 3D systems.

Let r_0 stand for a point of the system attractor and ε be a fixed positive number, not large in comparison to linear dimensions of the attractor. The points x_0, y_0 and z_0 are chosen so that the perturbation vectors $\Delta x_0 = x_0 - r_0$, $\Delta y_0 = y_0 - r_0$, $\Delta z_0 = z_0 - r_0$ have the length ε and are mutually

orthogonal. After a certain small time interval T, the points r_0, x_0, y_0 and z_0 are transformed into points r_1, x_1, y_1 and z_1, respectively. Then, new perturbation vectors $\Delta x_1 = x_1 - r_1$, $\Delta y_1 = y_1 - r_1$, $\Delta z_1 = z_1 - r_1$ are considered. The orthogonlization using the well-known (in linear algebra) Gramm-Schmidt method is carried out. After this step, the obtained vectors of perturbation $\Delta x_1'', \Delta y_1'', \Delta z_1''$ become orthonormalized, i.e. they are mutually orthogonal and have the unit length. Then, the renormalization of the perturbation vectors is carried out again to get lengths of the vectors in terms of the magnitude ε:

$$\Delta x_1''' = \Delta x_1'' \cdot \varepsilon, \ \ \Delta y_1''' = \Delta y_1'' \cdot \varepsilon, \ \Delta z_1''' = \Delta z_1'' \cdot \varepsilon. \tag{10}$$

We take the following perturbed points

$$x_1' = x_1 + \Delta x_1''', \ y_1' = y_1 + \Delta y_1''', \ z_1' = z_1 + \Delta z_1'''. \tag{11}$$

Next, the process is repeated, i.e. instead of the points r_0, x_0, y_0 and z_0, the points r_1, x_1', y_1' and z_1' are taken into account, respectively.

Repeating the so far described procedure M times, one computes

$$S_1 = \sum_{k=1}^{M} \ln\|\Delta x_k'\|, \ S_2 = \sum_{k=1}^{M} \ln\|\Delta y_k'\|, \ S_3 = \sum_{k=1}^{M} \ln\|\Delta z_k'\|. \tag{12}$$

Then, a spectrum $\Lambda = \{\lambda_1, \lambda_2, \lambda_3\}$ of LEs can be found by the following formulas:

$$\lambda_i = \frac{S_i}{MT}, \quad i = 1, 2, 3. \tag{13}$$

In this method, the choice of time interval T plays a crucial role. Indeed, if one takes too large time interval T, then all perturbed trajectories will be inclined in the direction corresponding to the maximum LE, and hence the obtained results will not be reliable.

3.2. Wolf method [1]

In reference [1], a novel algorithm to find nonnegative Lyapunov exponents by using a time series was proposed. It was illustrated that the Lyapunov exponents are associated with either exponential divergence or convergence of the neighborhood orbits in the considered phase space. In general, the method is applicable only when analytical governing equations are known, and it is based on tracing the large time-consuming increase in the number of elements in a small volume of an attractor.

We defined a Lyapunov exponent and a spectrum of Lyapunov exponents, and then illustrated how the system dynamics depends on the number of exponents with different signs in the spectrum. Our approach included reconstruction of an attractor and investigation of orbital divergence on the possibly smallest distances using the approximate Gramm-Schmidt orthogonalization procedure in the reconstructed phase. In order to estimate the largest Lyapunov exponent, a long trace of time evolution of the chosen pair of the neighborhood orbits was carried out. In general, a particular attention should be paid, since the reconstructed attractor may contain points belonging to different attractors.

Two versions of the method are proposed. The first one includes the so-called fixed evolution time, where the time interval associated with the change of the points is fixed.

The main idea of the proposed method is as follows: the largest Lyapunov exponent is computed based on one time series and used when the equations describing the system evolution are unknown and when it is impossible to measure all remaining phase coordinates.

Consider a time series $x(t), \ \ t = 1, ..., N$ of one coordinate of a chaotic process measured in equal time intervals. The method of mutual information allows one to define the time delay τ, whereas the method of false neighbors yields the dimension of the embedded space m. As a result of the reconstruction, one gets a set of points of the space R^m:

$$x_i = (x(i), x(i-\tau), ..., x(i-(m-1)\tau)) = (x_1(i), x_2(i), ..., x_m(i)), \tag{14}$$

where $i = ((m-1)\tau + 1), ..., N$.

We take a point from the series (3) and denote it by x_0. In the series (3), one can find a point $\%_0$, where the relation $\| \%_0 - x_0 \| = \varepsilon_0 < \varepsilon$ holds, and where ε is a fixed quantity, essentially less

than the dimension of the reconstructed attractor. It is required that the points x_0 and x_0' are separated in time. Then, time evolution of these points on the reconstructed attractor is observed until the distance between points achieves $\varepsilon_{\max}$. The new points are denoted by x_1 and x_1', the distance is ε_0', and the associate interval of time evolution is denoted by T_1.

After that, we again consider the sequence (14) the find the point x_p' located close to x_1, where $\| x_p' - x_1 \| = \varepsilon_1 < \varepsilon$ holds. Vectors $x_p' - x_1$ and $x_p' - x_1$ should possibly have the same direction. Then, the procedure is repeated for points x_1 and x_1'.

By repeating the above-described procedure M times, the largest Lyapunov exponent is estimated:

$$\lambda \cong \sum_{k=0}^{M-1} \ln(\varepsilon_k' / \varepsilon_k) / \sum_{k=1}^{M} T_k. \quad (15)$$

This method was employed in the present research for testing the accuracy of results by using the classical and known spectra of the Lyapunov exponents of the Hénon map, Rössler equations, chaos and hyperchaos exhibited by the Lorenz system, and McKay-Glass equation [29]. In addition, the method has been also employed to study the Belousov-Zhabotinsky reaction [30] and the Couette-Taylor flow [31].

Wolf et al. [1] pointed out certain restrictions on the choice of the embedding dimension and magnitude of time required for the attractor reconstruction to achieve the most accurate estimate of the Lyapunov exponents. Using the Rössler attractor [11] and the Belousov-Zhabotynskiy reaction [30], the authors demonstrated the effects of the time change during the attractor reconstruction, time of evolution of the system between steps of the time change, the maximum length of the replacement vector and the minimum length of the exchange vector on the values of the estimated largest Lyapunov exponent. Furthermore, it was shown that variation of the time of the system evolution between 0.5 and 1.5 leads to reliable estimates of the studied three chaotic attractors. Also, some data requirements that make it possible to obtain the most accurate estimate of the Lyapunov exponent, such as the use of small length scale data as well as some restrictions on the presence of noisy perturbations in the data (static and dynamic), were discussed.

The proposed algorithms can be used to detect chaos as well as to compute its parameters also for the experimental data with a few positive exponents. Furthermore, numerical studies have shown that the deterministic chaos can be distinguished from white noise (the Belousov-Zhabotinsky reaction) and have presented the topological complexity of chaos (the Lorenz attractor).

3.3. Rosenstein method [2]

Despite this method is simple in realization compared to the previous ones and it is characterized by high computational speed, it does not directly yield λ_1, but rather the function

$$y(i, \Delta t) = \frac{1}{\Delta t} \left\langle \ln d_j(i) \right\rangle, d_j(i) = \min_{x_j} \| x_j - x_j' \|, \quad (16)$$

where x_j is a given point, and x_j' denotes its neighbor.

The algorithm is based on the relationship between d_j and the Lyapunov exponents: $d_j(i) \approx e^{\lambda_1 (i \Delta t)}$. The largest Lyapunov exponent is computed by estimating the inclination of the most linear part of the function. It should be mentioned that finding this linear part does not belong to easy tasks.

3.4. Kantz method [3]

The algorithm proposed by Kantz [3] computes the LLE by searching all neighbors in vicinity of the reference trajectory and estimates the average distance between neighbors and the reference trajectory as a function of time (or a relative time multiplied by the data sampling frequency). The algorithm is based on the following formula

$$S(\tau) = \frac{1}{T} \sum_{t=1}^{T} \ln \left(\frac{1}{|U_t|} \sum_{i \in U_t} |x_{t+\tau} - x_{i+\tau}| \right), \quad (17)$$

Preprints (www.preprints.org) | NOT PEER-REVIEWED | Posted: 17 January 2018 doi:10.20944/preprints201801.0154.v1

Peer-reviewed version available at Entropy 2018, 20, 175; doi:10.3390/e20030175

where x_t stands for an arbitrary signal point; U_t is a neighborhood of x_t; x_i is a neighbor of x_t; τ – relative time multiplied by the sampling frequency; T – sample size; $S(\tau)$ – stretching factor in the region of a linear growth indicating a curve whose slope is equal to LE, i.e. $e^{\lambda\tau} \propto e^{S(\tau)}$. However, the assumption of a linear growth introduces new errors. Despite the fact that the method is useful and accurate for systems with known LEs, the choice of parameters and the region where the mentioned linear growth occurs is, in practice, arbitrary.

The method yields correct results if the value of the Lyapunov exponent is known a priori, and hence the space with the tangent equal to that value can be chosen.

3.5. Computation of LLE based on synchronization of nonnegative feedback [6, 7]

In reference [6], the method of LLE computation based on synchronization of coupled identical systems was proposed. The following k-dimensional discrete system:

$$y_i' = f(y_i) \tag{18}$$

was considered, where $y \in \mathbb{R}^k$, $i \in (1, 2, \dots, k)$. The supplemental system was proposed in the following way

$$x_i' = f(y_i + \Delta y_i), \tag{19a}$$

$$y_i' = f(y_i), \tag{19b}$$

$$\Delta y_i' = [f(y_i + \Delta y_i) - f(y_i)] \exp(-p), \tag{19c}$$

where $x, y, \Delta y \in \mathbb{R}^k$. Evolution of k-dimensional system is governed by k of LLEs. Consequently, synchronization of the perturbed and nonperturbed systems (19a) and (19b) is guaranteed by the following inequality

$$p > \lambda_{max}, \tag{20}$$

where λ_{max} stands for LLEs of the studied systems (18).

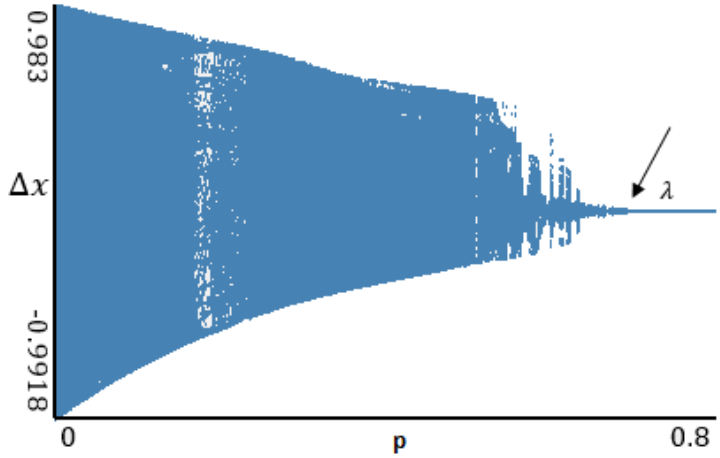

Figure 1. Synchronization for the case of logistic map

In reference [7], systems with excitations are studied. The authors proposed the following way of coupling of identical systems:

$$\dot{x} = f(x), \tag{21a}$$

$$\dot{y} = f(y) + d(x - y). \tag{21b}$$

The presented approach is limited to application to the systems with known equations of evolutions, and the way of introducing the coupling of two identical systems depends on the considered system type.

3.6. Jacobi method [32, 33]

This method has been proposed in references [32, 33]. Its main idea is to use an algorithm, the scheme of which is illustrated in Fig. 2. A sphere of small radius ε is taken. After a few iterations m, a certain operator T^m transforms this sphere into an ellipsoid having $a_1, \dots, a_p$ half-axes. The sphere is stretched along the axes $a_1, \dots, a_s > \varepsilon$, where s is the number of positive LEs. For sufficiently small ε, the operator T^m is close to the sum of the shear operator and the linear operator A. The LLEs are computed as averaged eigenvalues of the operator A on the whole attractor.

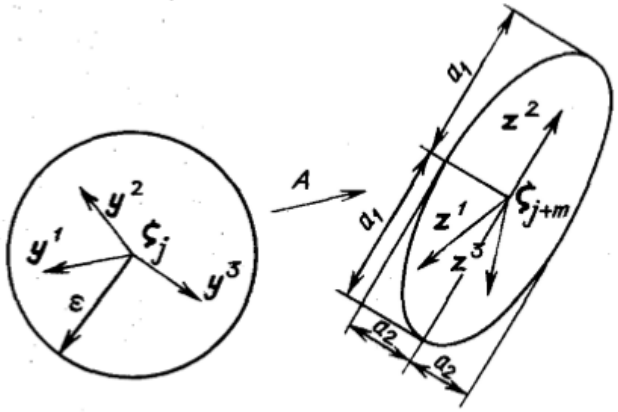

Figure 2. Transformation of a sphere of small radius into a counterpart ellipsoid

A vector ς_j is chosen, and a set $\{\varsigma_{k_i}\}(i = 1, \dots, N)$ of i-th neighborhood vectors is found. The following set of vectors $y_i \equiv \varsigma_{k_i} - \varsigma_j$, where $\|y_i\| \le \varepsilon$, is taken. After m successive iterations, the operator T^m transforms the vector ς_j into ς_{j+m}, and the vector ς_{k_i} into $\varsigma_{k_{i+m}}$. Consequently, the vectors y_i are transformed into

$$y_{i+m} = \varsigma_{k_{i+m}} - \varsigma_{j+m}.$$

Assuming that the radius ε is sufficiently small, one can introduce the operator A_j as follows

$$y_{i+m} = A_j y_i.$$

The operator A_j describes the system in variations. To estimate the operator A, the least-square method can be employed:

$$\min_{A_j} S = \min_{A_j} \frac{1}{N} \sum_{i=0}^{N} (y_{i+m} - A_j y_i)^2.$$

This yields the following system of equations of the dimension $n \times n$:

$$A_j V = C, (V)_{kl} = \frac{1}{N} \sum_{i=1}^{N} y_i^k y_i^l,$$

$$(C)_{kl} = \frac{1}{N} \sum_{i=1}^{N} y_{i+m}^k y_i^l,$$

where V, C are the matrices of the dimension $n \times n$, y_i^k stands for the k-th component of vector y_i, and y_{i+m}^k is the k-th component of the vector y_{i+m}. If A is a solution to the mentioned equations, then the LEs can be found in the following way

$$\lambda_i = \lim_{n \to \infty} \frac{1}{n\tau} \sum_{j=1}^{n} \ln A_j e_i^j,$$

where $\{e_j\}$ is a set of basic vectors in tangent space ς_j.

The algorithm can be realized in a way similar to the computation of LEs of the ODEs given analytically.

Preprints (www.preprints.org) | NOT PEER-REVIEWED | Posted: 17 January 2018 doi:10.20944/preprints201801.0154.v1

Peer-reviewed version available at Entropy 2018, 20, 175; doi:10.3390/e20030175

Let us choose an arbitrary basis $\{e^s\}$ and then follow the changes in the length of the vector $A_j e^s$. As the vectors $A_j e^s$ grow and their orientations change, it is necessary to perform their orthogonalization and normalization by using, for example, the Gramm-Schmidt procedure. Then, the procedure is repeated for the new basis.

The mentioned method allows one to estimate a spectrum of nonnegative LEs. However, the method has a serious disadvantage - it is highly sensitive to noise and errors.

3.7. Modification of the neural network method [4, 5]

We proposed a novel and counterpart method to compute LEs based on a modification of the neural network method (see Fig. 3)

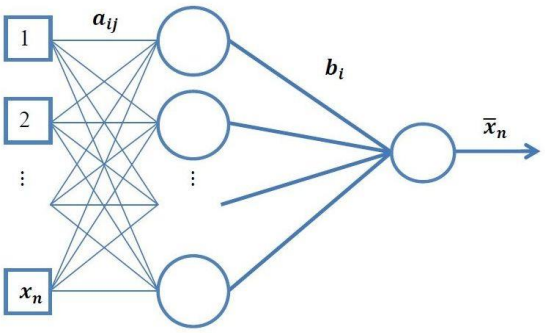

Figure 3. One-layer neutral network

To realize the neural network algorithm, the following criteria were taken into account:

(i) the network is sensitive to the input information (information is given in the form of real numbers);

(ii) the network is self-organizing, i.e. it yields the output space of solutions only based on the inputs;

(iii) the neural network is a network of straight distribution (all connections are directed from input neurons to output neurons);

(iv) owing to the synapses tuning, the network exhibits dynamics couplings (in the learning process, the tuning of the synaptic coupling takes place $(dW / dt \neq 0)$, where W stands for the weighted coefficients of the network).

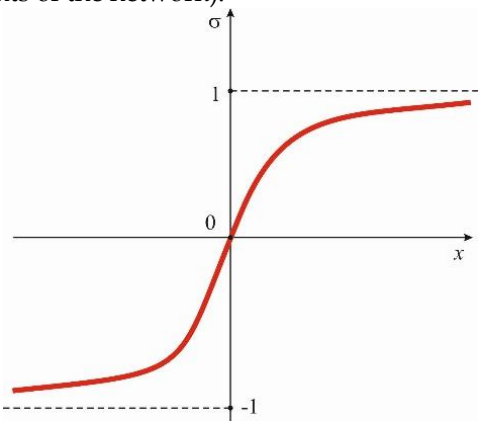

Figure 4. Transition function

In the network, there is a hidden layer of neurons, which contains the hyperbolic tangent playing a role of an activation function (Fig. 4).

A derivative of the hyperbolic tangent is described by a quadratic function, as it is in the case of a logistic function. However, in contrast to the logistic function, the space of the values of the hyperbolic tangent falls within the interval (-1;1). This results in higher convergence in comparison to the standard logistic function.

Prognosis of $\hat{x}_k$ of a scalar time series x_k is made by employing the following formula

Preprints (www.preprints.org) | NOT PEER-REVIEWED | Posted: 17 January 2018 doi:10.20944/preprints201801.0154.v1

Peer-reviewed version available at Entropy 2018, 20, 175; doi:10.3390/e20030175

$$\hat{x}_k = \sum_{i=1}^{n} b_i \tanh\left(a_{i0} + \sum_{j=1}^{d} a_{ij} x_{k-j}\right), \quad (22)$$

where n stands for the number of neurons, d is the number of the searched LE, a_{ij} stands for the $n \times (d+1)$ matrix of coefficients, and b_i is the vector of length n. The matrix a_{ij} contains the coupling forces with respect to the network input and the vector b_i is used to control the input of each neuron to the network output, whereas the vector a_{i0} is used for relatively simple learning based on data with nonzero averaged value.

Weights a and b are chosen in a probabilistic way, and the dimension of the searched solution is decreased in the process of learning. The associated Gaussian is chosen in a way to have initial standard distribution 2^{-j}, centered with respect to zero in order to promote the most recent time delays (small values of j) in the phase space. The coupling forces are chosen in a way to minimize the averaged one step mean square error of a forecast

$$e = \frac{\sum_{k=d+1}^{c} (\hat{x}_k - x_k)^2}{c-d}. \quad (23)$$

When the network is being trained, sensitivity of the output is defined in each time step by computing partial derivatives of all averaged points of the time series in each time step x_{k-j}:

$$\hat{S}(\mathrm{j}) = \frac{1}{c-j} \sum_{k=j+1}^{c} \left| \frac{\partial \hat{x}_k}{\partial x_{k-j}} \right|. \quad (24)$$

In the case of the network given by (22), the partial derivatives have the following form

$$\frac{\partial \hat{x}_k}{\partial x_{k-j}} = \sum_{i=1}^{n} a_{ij} b_i \operatorname{sech}^2 \left(a_{i0} + \sum_{m=1}^{d} a_{im} x_{k-m} \right). \quad (25)$$

The largest value j is the optimal embedding dimension, and the key role is played by $\hat{S}(\mathrm{j})$ as in the false nearest neighbors method. The individual values of $\hat{S}(\mathrm{j})$ yield a quantitative estimate of the importance of each time step using the associated terms of the autocorrelation function or coefficients of the associated linear model.

The weight coefficients of the trained neural network are substituted to the matrix of solutions, and the input data are used to define the initial state. The computation of the spectrum is realized by employment of the generalized Benettin algorithm based on the obtained system of equations.

4. Wavelet methods

4.1. Gauss wavelets [13]

In the majority of engineering problems, the Fourier analysis is insufficient, since it deals with the averaged spectrum of the whole studied vibration signal and presents only a general picture of the signal. On the contrary, wavelets play a role of a microscope, which allows one to observe the spectrum at each time instant, and hence to detect a birth/death of the frequencies in time.

A wavelet transform of a 1D signal consists of its development with respect to a basis being usually a soliton-like function with given properties. The basis is obtained by displacement and tension/compression of a function, called a wavelet.

In the present work, the Gauss wavelets, defined as derivatives of the Gauss function, were used. Higher-order derivatives have many zero moments, and hence they allow one to obtain information about higher-order features hidden in the investigated signal.

The 8th order Gauss wavelets of the of the following form were employed

$$g_8(x) = -(105 - 420x^2 + 210x^4 - 28x^6 + x^8) exp^{\frac{-x^2}{2}}. \quad (26)$$

5. Analysis of classical dynamical systems by LEs and Gauss wavelets

In this section, we study simple classical systems (Tables 1, 4, 7, 10, 13) with emphasis put on a comparison of the LEs (Tables 2, 5, 8, 11, 14) obtained using the Wolf, Rosenstein and Kantz and

Preprints (www.preprints.org) | NOT PEER-REVIEWED | Posted: 17 January 2018 doi:10.20944/preprints201801.0154.v1

Peer-reviewed version available at Entropy 2018, 20, 175; doi:10.3390/e20030175

neural network methods. The convergence of the mentioned methods, depending on the number of iteration steps, is illustrated and discussed (Tables 3, 6, 9, 12, 15).

5.1. Logistic map [10]

A logistic map describes how the population changes with respect to time

$$X_{n+1} = RX_n(1 - X_n). \quad (27)$$

Here, X_n takes the values from 0 to 1 and presents the population in the n-th year, whereas X_0 denotes the initial population (in the year 0); R is a positive parameter characterizing an increase in the population (computations were carried out for R = 4).

The first Lyapunov exponent and the Kaplan-Yorke dimension were estimated by Sprott [35]. He obtained: λ_1=0.693147181, and the Kaplan-Yorke dimension: 1.0.

Tables 1, 4, 7, 10, 13 report the following results: a) signal; b) signal window; c) Poincaré pseudo-map; d) Fourier power spectrum; e) Gauss 8 wavelet; f) bifurcation diagram with LLE; g) graphs of LEs on the control parameters plane.

Table 1. Nonlinear **c**haracteristics of the oscillation signal: (a) time histories; (b) time window; (c) Poincaré pseudo-map; (d) Fourier frequency spectrum; (e) wavelet spectrum; (f) bifurcation diagram and LLE; (g) no graph of Lyapunov exponents (logistic map)

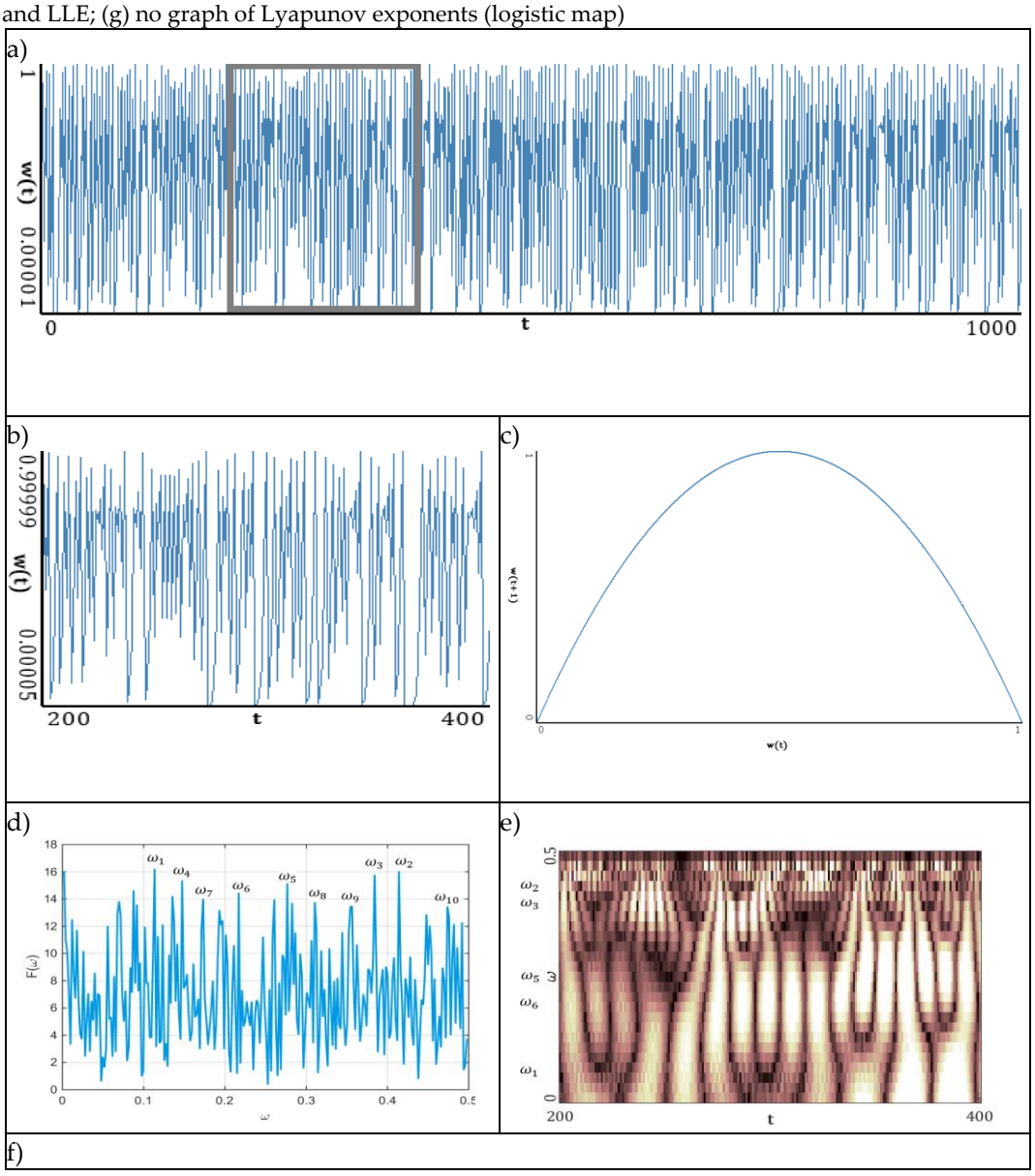

Preprints (www.preprints.org) | NOT PEER-REVIEWED | Posted: 17 January 2018 doi:10.20944/preprints201801.0154.v1

Peer-reviewed version available at Entropy 2018, 20, 175; doi:10.3390/e20030175

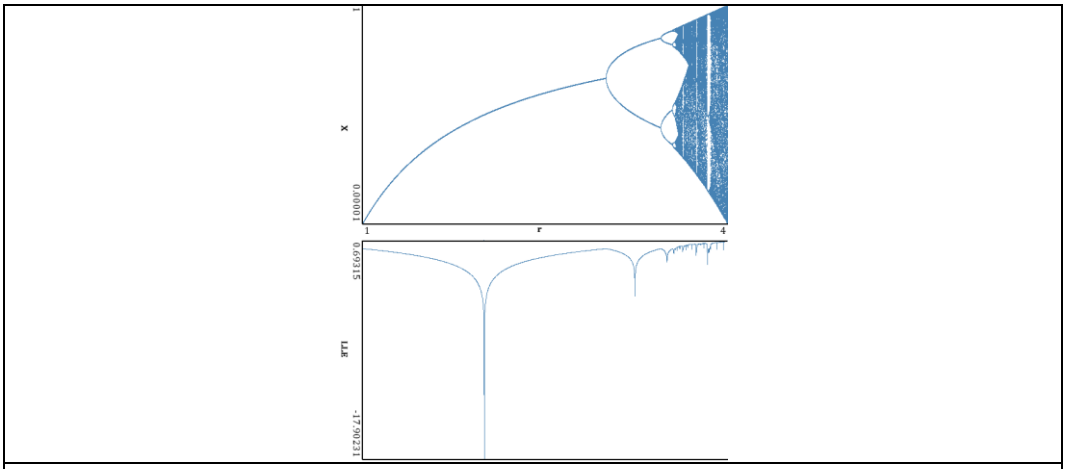

g) the system consists of one control parameter, and hence the graph of Lyapunov exponents cannot be constructed

Table 2. Spectrum of Lyapunov exponents and LLEs computed by different methods (logistic map)

LE spectrum			
Benettin method		Neural network	
(LEs): 0.69315 Dimension Kaplan-York (DKY): 1 Kolmogorov-Sinai entropy (KSE): 0.69315 Phase volume compression (PVC): 0.69315		LEs: 0.69290 DKY: 1 EKS: 0.69290 PVC: 0.69290	
LLE			
Wolf method	Rosenstein method	Kantz method	Method of synchronization
LLE: 0.99683	LLE: 0.690553	LLE: 0.31321	LLE: 0.696

Table 3. Fourier power spectra and Gauss wavelet spectra obtained for $\Delta t = 1, 2$ and the LLEs computed by different methods (logistic map)

$\Delta t = 1$	$\Delta t = 2$
Fourier power spectrum	
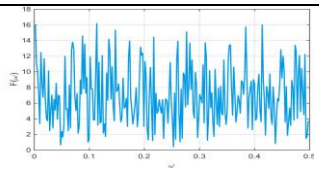	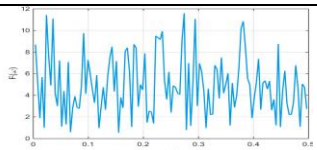
Gauss wavelet	
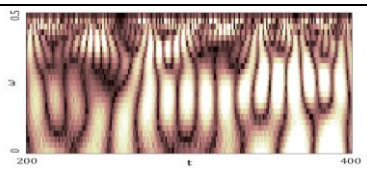	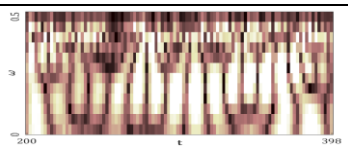
LLE (Wolf)	
0.99961	1.00014
LLE (Rosenstein)	
0.69231	0.69065
LLE (Kantz)	
0.31321	
LLE (Synchronization)	
0.69400	0.69330
LEs (Benettin)	
LES: 0.69318 DKY: 1.00000 KSE: 0.69318 PVC: 0.69318	LES: 0.69400 DKY: 1.00000 KSE: 0.69400 PVC: 0.69400
LEs (neural network)	
LES: 0.69290	LES: 0.69107

Preprints (www.preprints.org) | NOT PEER-REVIEWED | Posted: 17 January 2018 doi:10.20944/preprints201801.0154.v1

Peer-reviewed version available at Entropy 2018, 20, 175; doi:10.3390/e20030175

DKY: 1 KSE: 0.69290 PVC: 0.69290	DKY: 1.00000 KSE: 0.69107 PVC: 0.69107

The power spectrum is noisy and it is not possible to distinguish the dominating frequency. A similar situation is exhibited by the Gauss wavelet, where a large set of frequencies is visible. They are varied with respect to power, the whole interval of the signal changes, and the estimated LLEs correlate with the bifurcation diagram for the same interval of the control parameter *r*.

As can be seen in Table 2, all computational methods were compared with Benettin's original results. Good coincidence was exhibited by the neural network method, the Rosenstein method and the method of synchronization. Kantz/Wolf method gave decreased/increased value of LLE in comparison to the original value.

5.2. Hénon map [8]

The Hénon map takes a point (X_n, Y_n) and maps it into another point by the following formulas

$$\begin{aligned} X_{n+1} &= 1 - aX_n^2 + Y_n, \\ Y_{n+1} &= bX_n. \end{aligned} \tag{28}$$

The following parameters are fixed for numerical experiments: $a = 1.4$, $b = 0.3$. Since the equations (28) do not correspond to a real object, the parameters are replaced with fixed values. Sprott [34] computed the Lyapunov spectrum and the Kaplan-Yorke dimension of the map using the Benettin method [17] by solving (28). He obtained the following LEs: $\lambda_1 = 0.419217$, $\lambda_2 = -1.623190$, and the Kaplan-Yorke dimension: 1.258267.

Table 4. Characteristics of the Hénon map: (a) time history; (b) time window; (c) Poincaré pseudo-map; (d) Fourier frequency spectrum; (e) wavelet spectrum; (f) bifurcation diagrams and LLEs; (g) graph of Lyapunov exponents

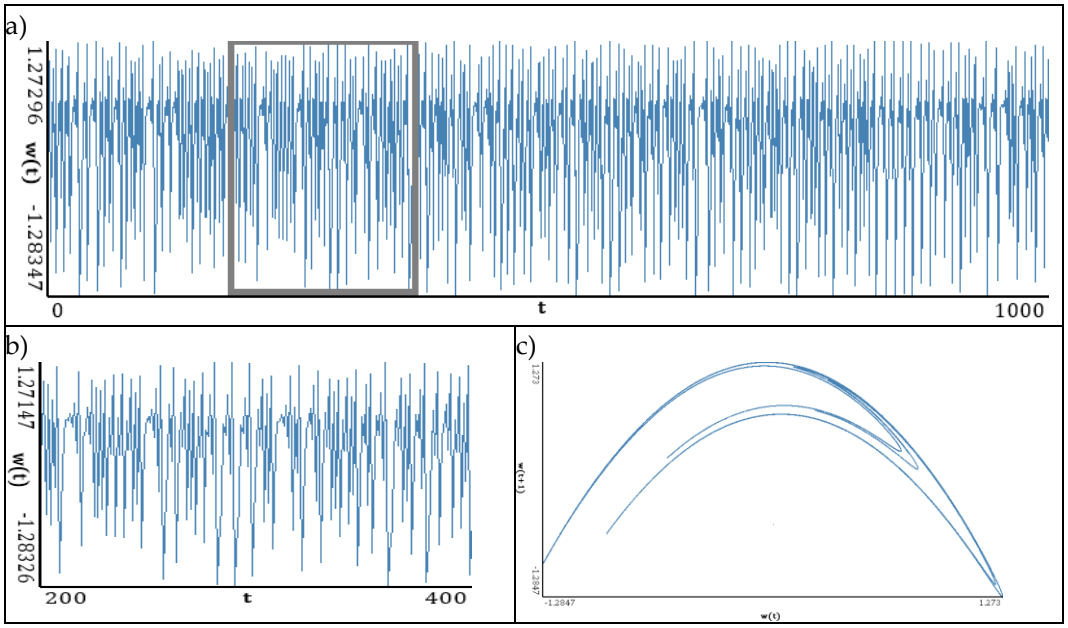

Preprints (www.preprints.org) | NOT PEER-REVIEWED | Posted: 17 January 2018 doi:10.20944/preprints201801.0154.v1

Peer-reviewed version available at Entropy 2018, 20, 175; doi:10.3390/e20030175

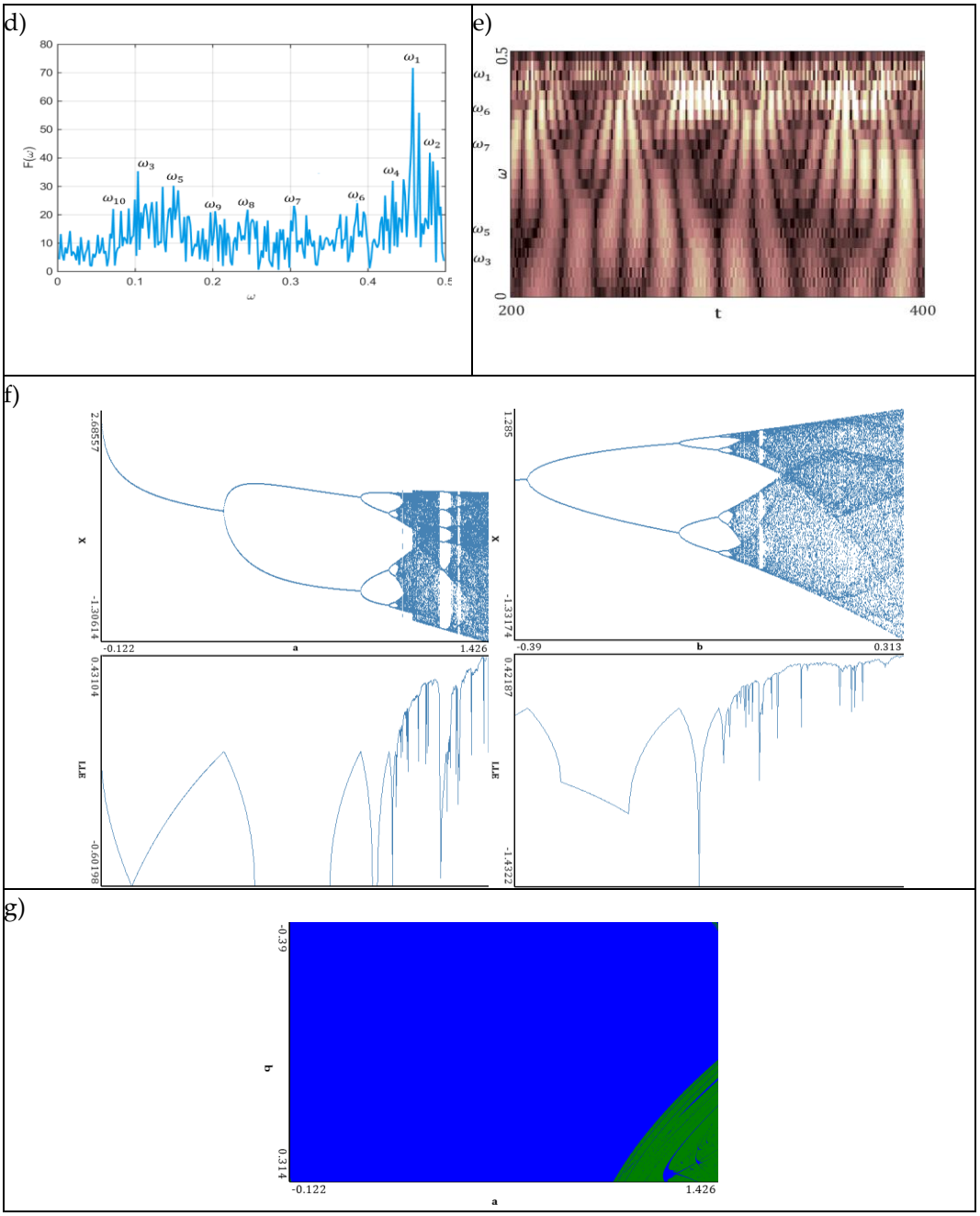

Similarly to the logistic map, the power spectrum exhibits a uniform noisy shape. However, one can distinguish a dominating frequency ($\omega_1 \approx 0{,}45$). It is also visible on the wavelet spectrum as a region of the largest amplitudes along the whole signal. Plots of the change in the LLE correlate with bifurcation diagrams for the same interval of changes in the parameters a and b. Dynamics of the LLE changes increases with the increase in both control parameters. Starting with the graphs of LEs for a given set of control parameters, the system mainly remains in a periodic regime, but it exhibits chaotic dynamics for large values of the control parameters.

Preprints (www.preprints.org) | NOT PEER-REVIEWED | Posted: 17 January 2018 doi:10.20944/preprints201801.0154.v1

Peer-reviewed version available at Entropy 2018, 20, 175; doi:10.3390/e20030175

Table 5. Lyapunov exponents spectrum and LLEs computed by different methods (Hénon map)

Spectrum of LLEs			
Benettin method		Neural network	
LEs: 0.41919 -1.62316 DKY: 1.25826 EKS: 0.41919 PVC: -1.20397		LEs: 0.41919 -1.62316 DKY: 1.25826 EKS: 0.41919 PVC: -1.20397	
LLEs			
Wolf method	Rosenstein method	Kantz method	Synchronization method
LLE: 0.38788	LLE: 0.414218	LLE: 0.17759	LLE: 0.40608

Beginning from the results shown in Table 5, the majority of the employed computational methods yielded good results. However, the most accurate results were obtained by the neural network method (for whole spectrum of LEs), the Rosenstein method, and the method of synchronization (in the case of LLEs). The Wolf and Kantz methods gave decreased estimated values of the LLEs.

Table 6. Fourier power spectra and Gauss wavelet spectra obtained for $\Delta t = 1, 2$ and the computed LLEs by different methods (Hénon map)

$\Delta t = 1$	$\Delta t = 2$
Fourier power spectrum	
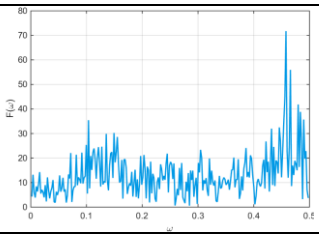	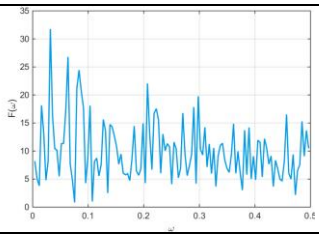
Gauss wavelet	
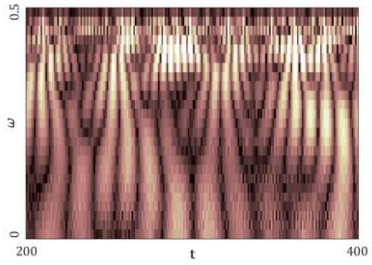	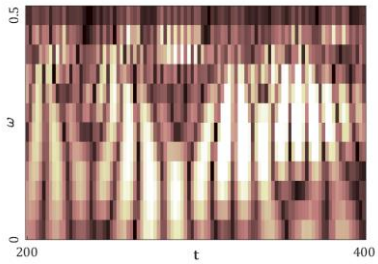
LLE (Wolf)	
0.4158	0.39734
LLE (Rosenstein)	
0.41637	0.400635
LLE (Kantz)	
0.17759	0.105365
LLE (synchronization)	
0.40608	0.40510
All LEs (Benettin)	
LEs: 0.41919 -1.62316 DKY: 1.25826 EKs: 0.41919 PVC: -1.20397	LEs: 0.41917 -1.62315 DKY: 1.25825 EKs: 0.41917 PVC: -1.20397
All LEs (neural network)	
LEs: 0.41919 -1.62316 DKY: 1.25826	LEs: 0.40924 -1.61321 DKY: 1.25368

Preprints (www.preprints.org) | NOT PEER-REVIEWED | Posted: 17 January 2018 doi:10.20944/preprints201801.0154.v1

Peer-reviewed version available at Entropy 2018, 20, 175; doi:10.3390/e20030175

KSE: 0.41919 PVC: -1.20397	KSE: 0.40924 PVC: -1.20397

5.3. *Hyperchaotic generalised Hénon map [9]*

To obtain the hyperchaotic Hénon map, one needs to take a point (X_n, Y_n, Z_n) and map it into the following one:

$$\begin{aligned} X_{n+1} &= a - aY_n^2 - bZ_n, \\ Y_{n+1} &= X_n, \\ Z_{n+1} &= Y_n. \end{aligned} \tag{29}$$

The computations were carried out for the following fixed parameters: $a = 3.4$, $b = 0.1$. The Lyapunov spectrum reported in reference [9] is: 0.276; 0.257; 4.040.

Table 7. Signal characteristics: (a) time history; (b) time window; (c) Poincaré pseudo-map; (d) Fourier frequency spectrum; (e) wavelet spectrum; (f) bifurcation diagram and LLE; (g) graph of Lyapunov exponents (generalized Hénon map)

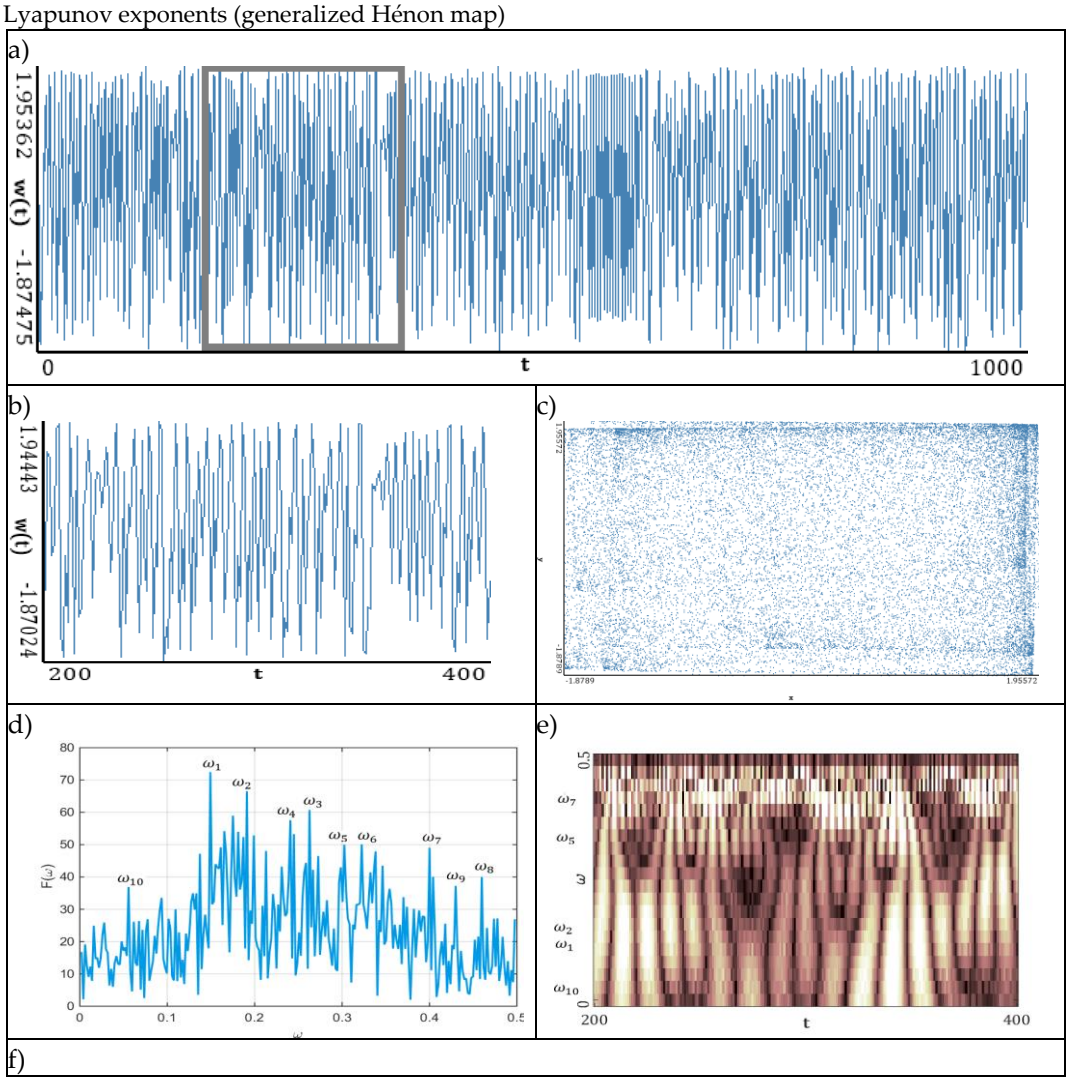

Preprints (www.preprints.org) | NOT PEER-REVIEWED | Posted: 17 January 2018 doi:10.20944/preprints201801.0154.v1

Peer-reviewed version available at Entropy 2018, 20, 175; doi:10.3390/e20030175

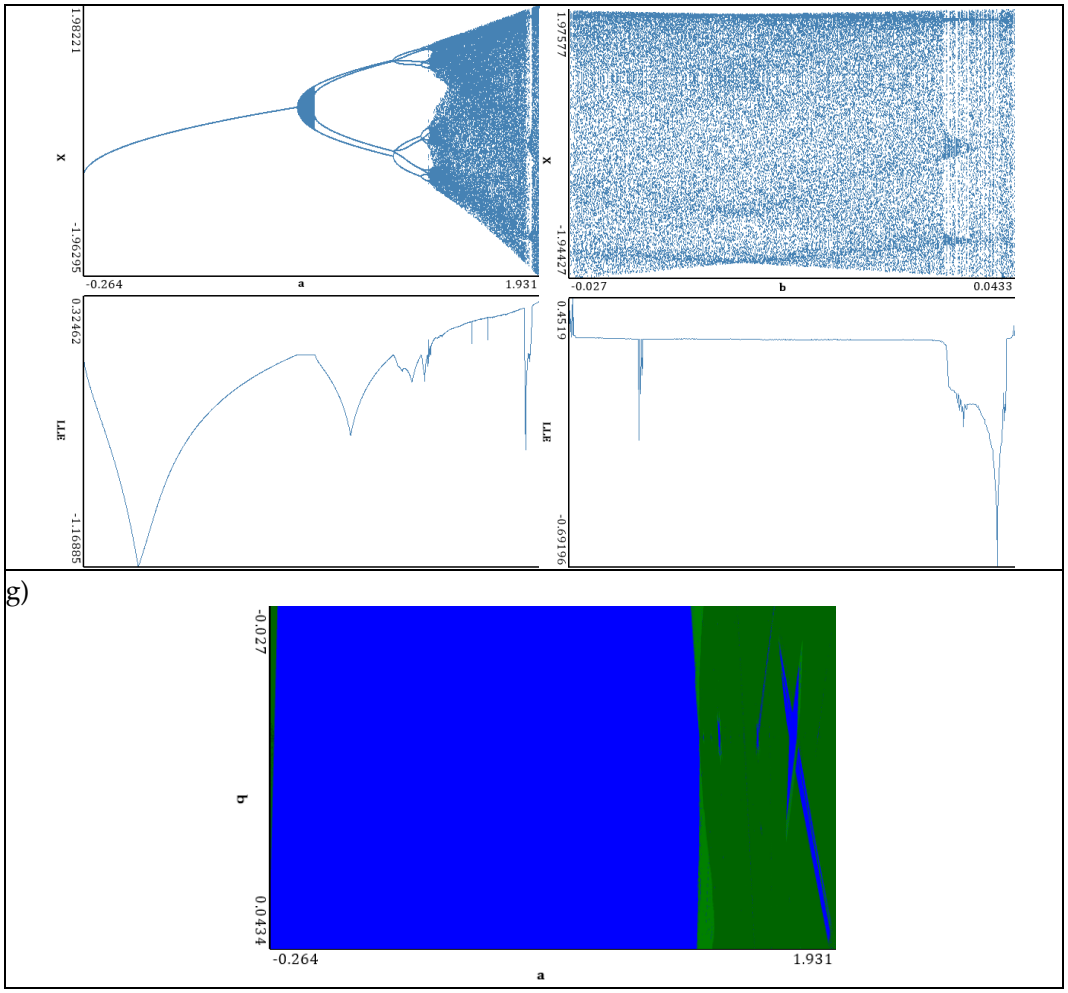

One can distinguish a large number of frequencies in the power spectrum. Frequencies with the largest amplitude are located in the interval [0.15; 0.3] (frequencies $\omega_1 - \omega_4$), but the remaining part of the spectrum is noisy. This interval corresponds to the brightest region on the Gauss wavelet, which is correlated with the values of the power spectrum. Changes in LLEs coincide with the bifurcation diagrams constructed for the same intervals of changes in the control parameters a and b. Dynamics of LLEs increases with the increase in the control parameters. As in the case of the Hénon map, the chart of LEs for the selected control parameters exhibits, for a majority of studied parameters, periodic dynamics. It transits into chaos for $a \approx 1.4$, and is almost suddenly shifted into hyper-chaos (2 positive LEs).

Table 8. Lyapunov exponents spectrum and LLEs computed by different methods (generalized Hénon map)

Spectrum of LEs			
Benettin method		Neural network	
LEs: 0.27628 0.25770 -4.04053 DKY: 2.13215 EKS: 0.53397 PVC: -3.50656		LEs: 0.29251 0.27104 -4.04583 DKY: 2.13929 EKS: 0.56355 PVC: -3.48227	
LLEs			
Wolf method	Rosenstein method	Kantz method	synchronization method
LLE: 0.45214	LLE: 0.27930	LLE: 0.26601	0.27250

Good results were obtained by the Benettin, Rosenstein and synchronization methods (divergence from the third decimal place). The neural network yielded slightly increased estimates

Preprints (www.preprints.org) | NOT PEER-REVIEWED | Posted: 17 January 2018 doi:10.20944/preprints201801.0154.v1

Peer-reviewed version available at Entropy 2018, 20, 175; doi:10.3390/e20030175

of two first LEs, whereas the third LE was estimated almost exactly. The Kantz method gave a decreased result in comparison to reference data. The Wolf method resulted in the largest error.

Table 9. Fourier power spectra and Gauss wavelet spectra obtained for $\Delta t = 1, 2$ and the computed LLEs by different methods (generalized Hénon map)

$\Delta t = 1$	$\Delta t = 2$
Fourier power spectrum	
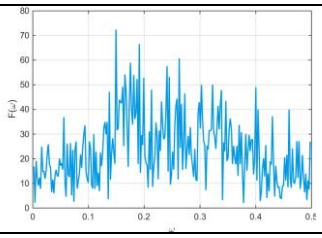	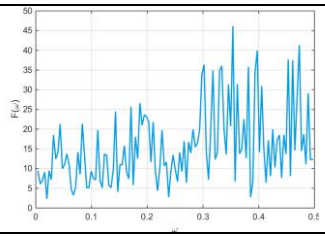
Gauss wavelet	
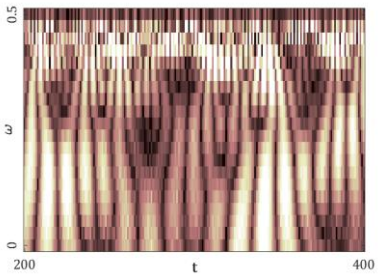	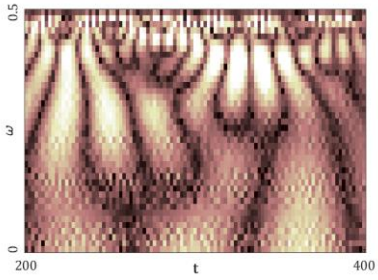
LLE (Wolf)	
0.45214	0.46706
LLE (Rosenstein)	
0.27930	0.27459 (0.62515)
LLE (Kantz)	
0.26601	
LLE (synchronization)	
0.27250	0.27200
All LEs (Benettin)	
LEs: 0.27628 0.25770 -4.04053 DKY: 2.13215 KSE: 0.53397 PVC: -3.50656	LEs: 0.27487 0.25631 -4.03774 DKY: 2.13155 EKS: 0.53118 PVC: -3.50656
All LEs (neural network)	
LEs: 0.29251 0.27104 -4.04583 DKY: 2.13929 KSE: 0.56355 PVC: -3.48227	LEs: 0.26304 0.24387 -4.14321 DKY: 2.12235 KSE: 0.50691 PVC: -3.63630

5.4. Rössler attractor [11]

The following Rössler system of ODEs was investigated

$$\begin{cases} \dot{x} = -y - z, \\ \dot{y} = x + ay, \\ \dot{z} = b + z(x - c), \end{cases} \tag{30}$$

and the computations were carried out for the following fixed parameters $a = b = 0.2$ and $c = 5.7$.

Preprints (www.preprints.org) | NOT PEER-REVIEWED | Posted: 17 January 2018 doi:10.20944/preprints201801.0154.v1

Peer-reviewed version available at Entropy 2018, 20, 175; doi:10.3390/e20030175

The original study yielded the Lyapunov spectrum: 0.0714, 0, -5:3943, and the Kaplan-Yorke dimension equal to 2.0132.

Table 10. Signal characteristics: (a) time history; (b) time window; (c) Poincaré pseudo-map; (d) Fourier frequency spectrum; (e) wavelet spectrum; (f) bifurcation diagrams and LLEs; (g) graphs of Lyapunov exponents (Rössler attractor)

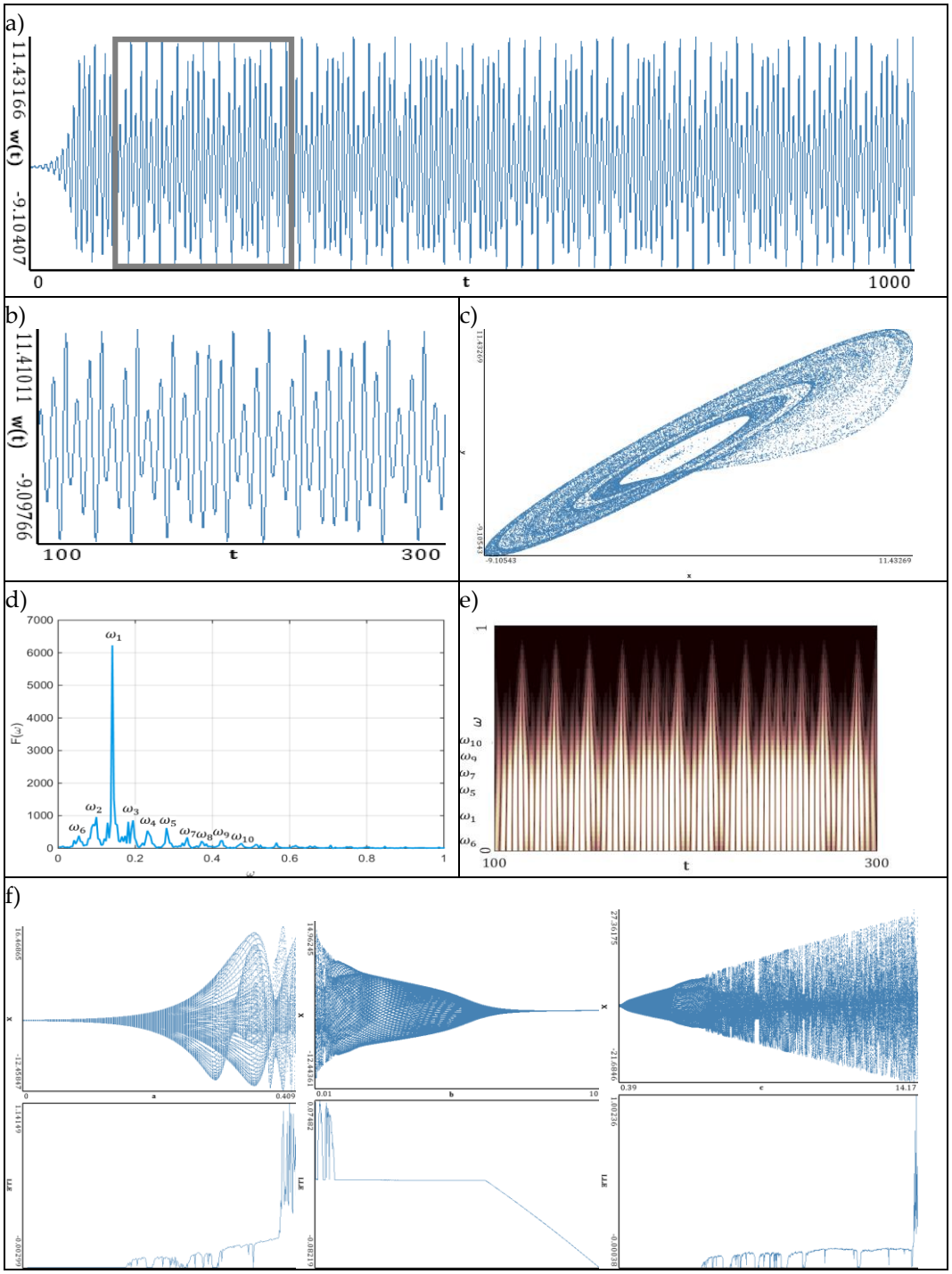

Preprints (www.preprints.org) | NOT PEER-REVIEWED | Posted: 17 January 2018 doi:10.20944/preprints201801.0154.v1

Peer-reviewed version available at Entropy 2018, 20, 175; doi:10.3390/e20030175

g)

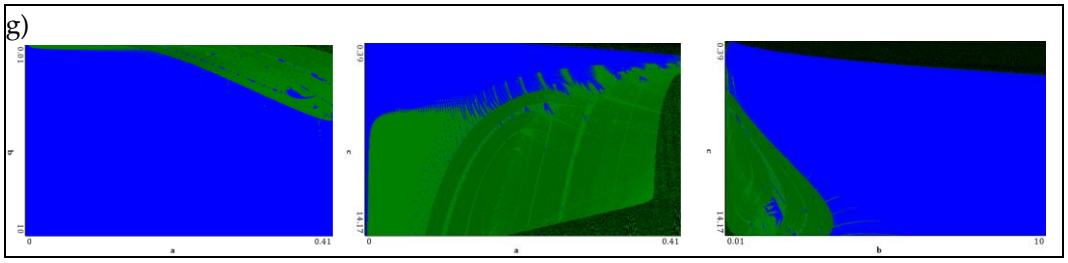

The power spectrum contains the fundamental frequency ω_1, which is accompanied by damped bursts (frequencies $\omega_2 - \omega_{10}$). In the whole time interval, the Gauss wavelet exhibits the brightest region of the fundamental frequency with darker peaks going to zero. Thus, the picture is analogous to the power spectrum. Contrarily to the studied maps, the bifurcation diagrams have a more complex structure. However, there is still correlation with the changes in LLEs for the corresponding control parameters. The parameter b has the most smallest influence on the change in LLE. Graphs of LLEs also exhibit a more complex structure. Borders of different vibration kinds have complex forms, which illustrates the increase in the system complexity. Aside from the chaos and hyper-chaos zones, there are drops of hyper hyper-chaos (3 positive LEs).

As far as Table 11 is considered, the best results were yielded by the Benettin and Rosenstein methods. The method of neural networks gave very good results in the case of estimates of two first LEs, but underestimated the third exponent. The Wolf method yielded smaller value of the first exponent compared to the reference data. The most underestimated results were given by the Kantz method.

Table 11. Lyapunov exponents spectrum and LLEs computed by different methods (Rössler attractor)

Spectrum of LEs		
Benettin method	Neural network	
LE: 0.07135 0.00000 -5.39420 DKY: 2.01323 KSE: 0.07135 PVC: -5.32285	LE: 0.07593 -0.00060 -0.78178 DKY: 2.09635 EKS: 0.07593 PVC: -0.70646	
LLEs		
Wolf method	Rosenstein method	Kantz method
LLE: 0.05855	LLE: 0.0726	LLE: 0.0208

Table 12. Fourier power spectra and Gauss wavelet spectra obtained for $\Delta t = 0.05, 0.1, 0.15, 0.2$ and the computed LLEs by different methods (Rössler attractor)

$\Delta t = 0.05$	$\Delta t = 0.1$	$\Delta t = 0.15$	$\Delta t = 0.2$
Fourier power spectrum			
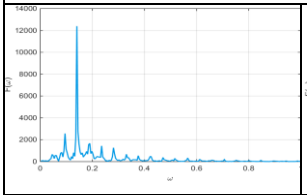	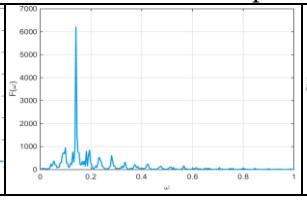	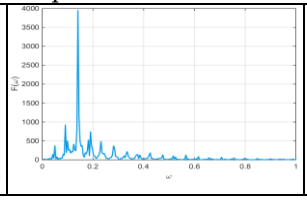	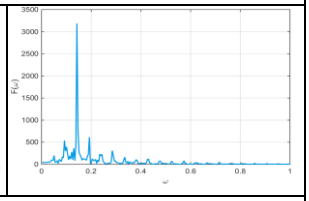
Gauss wavelets			

Preprints (www.preprints.org) | NOT PEER-REVIEWED | Posted: 17 January 2018 doi:10.20944/preprints201801.0154.v1

Peer-reviewed version available at Entropy 2018, 20, 175; doi:10.3390/e20030175

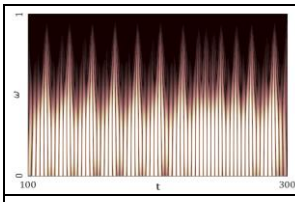	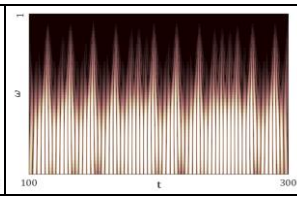	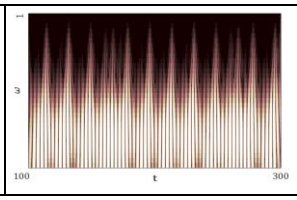	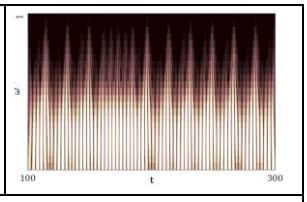
LLE (Wolf)			
	0.05855		
LLE (Rosenstein)			
0.083	0.0726	0.06553	0.606
LLE (Kantz)			
0.0234	0.0208	0.02133	0.0215
All LEs (Benettin)			
LES: 0.07156 0.00000 -5.38768 DKY: 2.01328 KSE: 0.07156 PVC: -5.31612	LES: 0.06959 0.00000 -5.21949 DKY: 2.01333 KSE: 0.06959 PVC: -5.14990	LES: 0.06789 0.00000 -4.34385 DKY: 2.01563 KSE: 0.06789 PVC: -4.27596	LES: 0.06205 -0.00001 -2.84111 DKY: 2.02184 KSE: 0.06205 PVC: -2.77906
All LEs (neural network)			
LES: 0.06259 -0.07984 -0.32528 DKY: 1.78396 KSE: 0.06259 PVC: -0.34253	LES: 0.07340 -0.02681 -0.23525 DKY: 2.19807 KSE: 0.07340 PVC: -0.18865	LES: 0.07374 0.00057 -0.36909 DKY: 2.20135 KSE: 0.07432 PVC: -0.29477	LES: 0.07983 -0.02816 -0.91182 DKY: 2.05667 KSE: 0.07983 PVC: -0.86015

The carried out numerical experiments showed that using the different sampling frequency, the power spectrum and wavelet spectrum were not changed. This was also validated by results obtained by the Benettin, neural networks and Rosenstein methods which yielded the results very close to original ones. The Kantz method gave underestimated results for different frequency selection, correlating with the results obtained for the standard sample size.

5.5. Lorenz attractor [12]

The input hydrodynamic system is governed by the following ODEs:

$$\begin{cases} \dot{x} = \sigma(y - x), \\ \dot{y} = x(r - z) - y, \\ \dot{z} = xy - bz, \end{cases} \tag{31}$$

where r stands for the normalized Rayleigh number (nondimensional number defining fluid behavior under gradient):

$$r = \frac{g\beta\Delta T L^3}{\nu\chi}. \tag{32}$$

In the above equation, the following notation is used: g – gravity of Earth; L - characteristic dimension of the fluid space; ΔT - temperature difference between fluid walls; ν - kinematic fluid viscosity, χ - thermal conductivity of the fluid; β - coefficient of heat fluid extension; σ - Prandtl number (takes into account heat source property) governed by the following equation

$$\sigma = \frac{\nu}{\alpha} = \frac{\eta C_p}{\aleph}, \tag{33}$$

where: $\nu = \eta / \rho$ - kinematic viscosity, η - dynamic viscosity, ρ - density, $\alpha = \frac{\aleph}{\rho C_p}$ - temperature transfer coefficient, $\aleph$ - heat transfer coefficient, C_p - specific heat capacity under constant pressure; and ρ - information about the geometry of the convective cell.

The following parameters were fixed: $\sigma = 10.0$, $r = 28.0$, $b = 8/3$. The original results follow: LEs: 0.9056, 0, -14.5723; the Kaplan-York dimension: 2.06215.

Preprints (www.preprints.org) | NOT PEER-REVIEWED | Posted: 17 January 2018 doi:10.20944/preprints201801.0154.v1

Peer-reviewed version available at Entropy 2018, 20, 175; doi:10.3390/e20030175

Table 13. Signal characteristics: (a) time history; (b) time window; (c) Poincaré pseudo-map; (d) Fourier frequency spectrum; (e) wavelet spectrum; (f) bifurcation diagrams and LLEs; (g) graphs of Lyapunov exponents (Lorenz attractor)

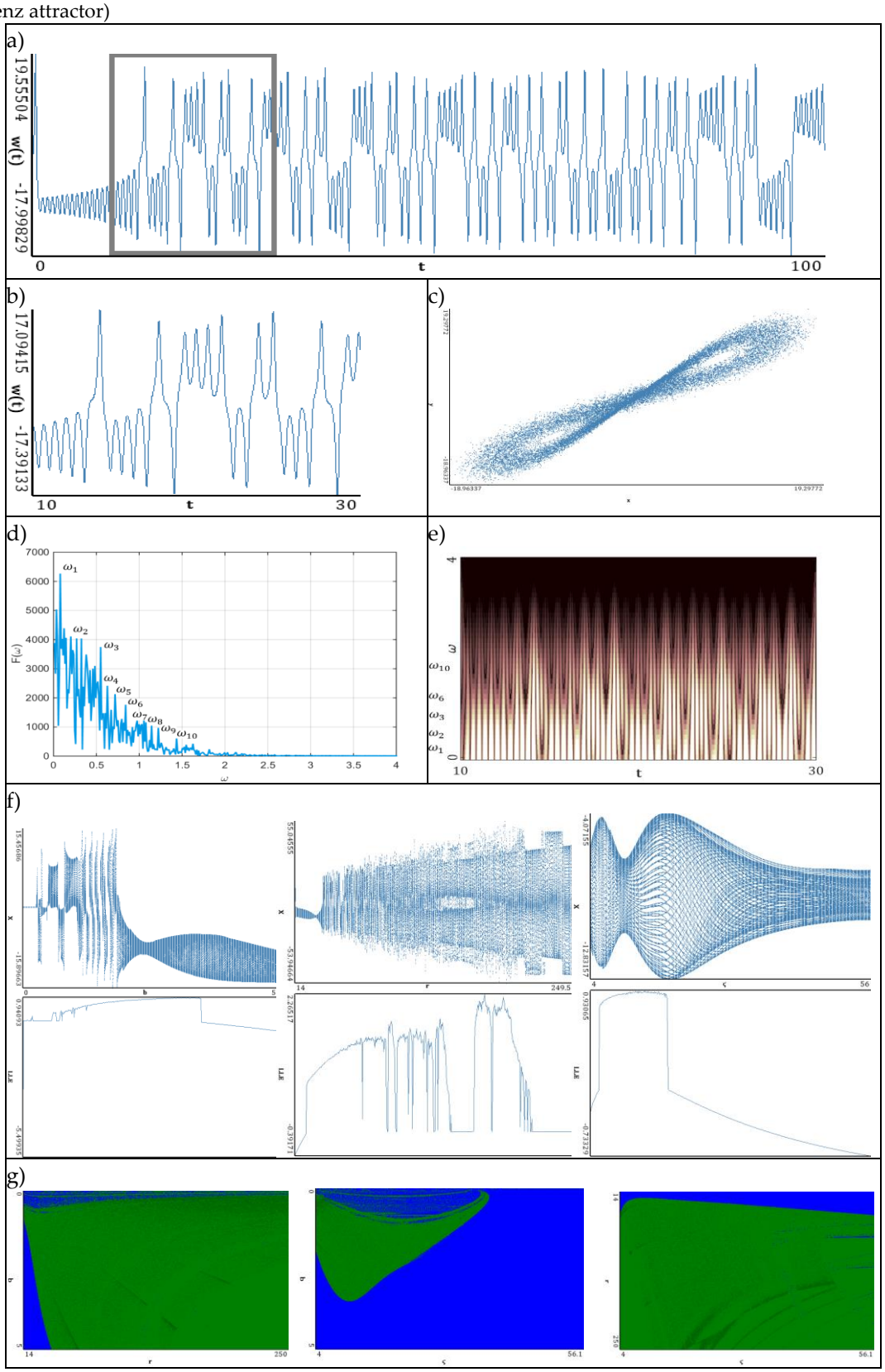

The power spectrum of the attractor uniformly decreases when approaching a finite frequency, and there is a lack of frequencies with a strongly dominating amplitude. The latter observation is also verified by the Gauss wavelet spectrum. The bifurcation diagrams, similar to those for the Rössler system, exhibit a complex structure, but the correlation to the LLEs change is conserved. The

Preprints (www.preprints.org) | NOT PEER-REVIEWED | Posted: 17 January 2018 doi:10.20944/preprints201801.0154.v1

Peer-reviewed version available at Entropy 2018, 20, 175; doi:10.3390/e20030175

richest/lowest dynamics of LLE is obtained for changing parameter r/σ. Based on the reported graphs of Les, one can conclude that the system dynamics is fully chaotic. There are also narrow windows of hyper-chaotic dynamics.

Table 14. Lyapunov exponents spectrum and LLEs computed by different methods (Lorenz attractor)

Spectrum of LEs		
Benettin method	Neural network method	
LE: 0.90557 0.00000 -14.57214 DKY: 2.06214 EKS: 0.90557 PVC: -13.66656	LE: 0.9490 0.0610 -13.9101 DKY: 2.07261 EKS: 1.0101 PVC: -12.9000	
LLEs		
Wolf method	Rosenstein methhod	Kantz method
LLE: 0.81704	LLE: 0.836	LLE: 0.807185

A comparison of the results reported in Table 14 with the original results exhibit an excellent coincidence of the Benettin method (original results) and the neural network method (+4.79%). The Wolf and Rosenstein methods yielded the underestimated results of the LLE value. The worst estimation was obtained by Kantz method.

Table 15. Fourier power spectra and Gauss wavelet spectra obtained for $\Delta t = 0.005, 0.01, 0.015, 0.02$ and the computed LLEs by different methods **(**Lorenz attractor)

$\Delta t = 0.005$	$\Delta t = 0.01$	$\Delta t = 0.015$	$\Delta t = 0.02$
Fourier power spectrum			
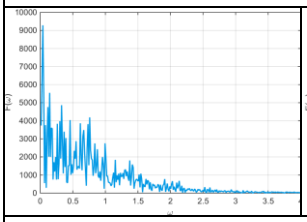	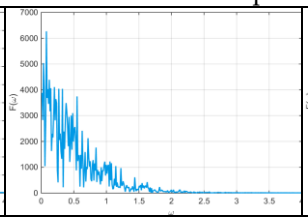	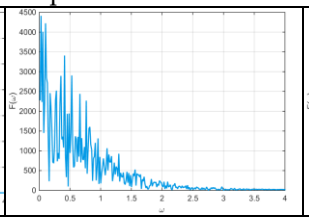	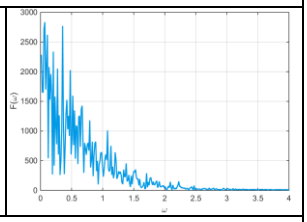
Gauss wavelet			
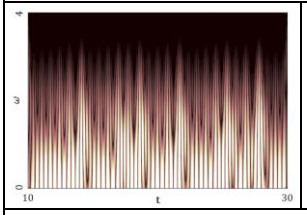	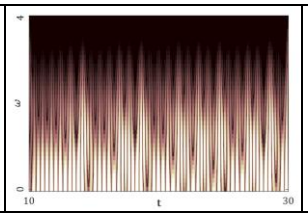	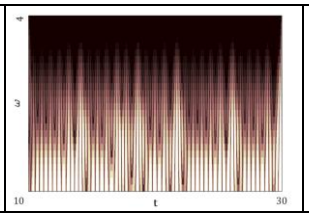	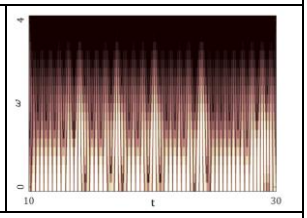
LLE (Wolf)			
	0.81704		
LLE (Rosenstein)			
0.876	0.836	0.858	0.859
LLE (Kantz)			
LES (Benettin)			
LES: 0.90632 0.00000 -14.57297 DKY: 2.06219 KSE: 0.90632 PVC: -13.66666	LES: 0.90523 0.00000 -14.57179 DKY: 2.06212 KSE: 0.90523 PVC: -13.66656	LES: 0.90551 0.00000 -14.57163 DKY: 2.06214 KSE: 0.90551 PVC: -13.66613	LES: 0.90596 0.00000 -14.57086 DKY: 2.06218 KSE: 0.90596 PVC: -13.66490
LES (neural network)			

	LE: 0.9490 0.0610 -13.9101 DKY: 2.07261 EKS: 1.0101 PVC: -12.9000		

Employing different sampling frequency does not change a picture of Fourier and wavelet power spectra. This was also validated by the Benettin and Rosenstein methods, which yield the results very close to the original values in spite of the arbitrary choice of the sampling frequency.

6. Concluding remarks

Analysis of the dynamics of the studied classical system by different methods leads to a conclusion that the most perspective and useful is the modified method of neural networks [4, 5]. It gives excellent convergence to the original results and, as the only one (besides of the Benettin method), allows to compute the spectrum of all Lyapunov exponents. In addition, very good results were obtained by the Rosenstein method for all studied systems. However, this method can be used to estimate only the largest Lyapunov exponents.

As far as convergence was considered, the Kantz method always yielded underestimated values, whereas the Wolf method gave either over- and underestimated values of LEs.

The method of synchronization worked reasonably well for the maps, but it was not useful in studying differential equations (the Rössler or Lorenz systems). The mentioned systems require the use of another type of coupling, which is a drawback of the method.

The carried out analysis of the works devoted to feasible methods for computation of Lyapunov exponents shows that there is no universal, verified and general method to compute the exact (in the sense of numerics) values of the Lyapunov exponents. This observation leads to the conclusion that there is a need to employ qualitatively different methods while checking the reliability of "true chaotic results". Furthermore, the analysis carried out in this paper is a helping tool to study systems of an infinite dimension. Such an analysis is the subject of the second paper part.

Acknowledgments: This work has been supported by the grants the Russian Science Foundation, RSF 16-19-10290.

Author Contributions: N.P. Erofeev, V. Dobriyan and M.A. Barulina performed the numerical study; A.V. Krysko and V.A. Krysko analyzed the obtained results; J. Awrejcewicz wrote the paper.

Conflicts of Interest: The authors declare no conflict of interest. The founding sponsors had no role in the design of the study; in the collection, analyses, or interpretation of data; in the writing of the manuscript, and in the decision to publish the results.

References

1. Wolf A., Swift J.B., Swinney H.L., Vastano J.A. Determining Lyapunov exponents from a time series. *Phys. D* **1985**, 16, 285-317.
2. Rosenstein M.T., Collins J.J., De Luca C.J. A practical method for calculating largest Lyapunov exponents from small data sets. *Phys. D* **1993**, 65, 117–134.
3. Kantz, H. A robust method to estimate the maximal Lyapunov exponent of a time series. *Phys. Lett. A* **1994**, 185, 77–87.
4. Dobriyan V., Awrejcewicz J., Krysko V.A., etc. On the Lyapunov exponents computation of coupled non-linear Euler-Bernoulli beams. *Proceedings of the Fourteenth International Conference on Civil, Structural and Environmental Engineering Computing*", Civil-Comp Press, Stirlingshire, UK, **2013,** Paper 53.
5. Krysko A.V., Awrejcewicz J., Kutepov I.E., Zagniboroda N.A., Dobriyan V., Krysko V.A. Chaotic dynamics of flexible Euler-Bernoulli beams. *Chaos* **2014**, 34(4), 043130-1 - 043130-25.
6. Stefański A. Estimation of the largest Lyapunov exponent in systems with impacts. *Chaos, Sol. Fract.* **2000**, 11(15), 2443-2451.

7. Stefański A., Kapitaniak T. Estimation of the dominant Lyapunov exponent of non-smooth systems on the basis of maps synchronization. *Chaos, Sol. Fract.* **2003**, 15(2), 233-244.
8. Hénon M. A two-dimensional mapping with a strange attractor. *Comm. Math. Phys.* **1976**, 50(1), 69–77.
9. Baier G., Klein M. Maximum hyperchaos in generalized Henon maps. *Phys. Lett. A* **1990,** 151(6-7), 281–284.
10. May, R. Simple mathematical model with very complicated dynamics. *Nature* **1976**, 261, 45–67.
11. Peitgen H.-O., Jürgens H., Saupe D. The Rössler Attractor. In *Chaos and Fractals: New Frontiers of Science.* Springer: Berlin, 2004, pp. 636–646.
12. Lorenz E.N. Deterministic nonperiodic flow. *J. Atm. Sci.* **1963,** 20(2), 130–141.
13. Astafeva N.M. Wavelet-analysis: basic theory and examples of applications. *Succ. Phys. Sci.* **1996,** 166(11), 1145–1170.
14. Awrejcewicz J., Kudra G., Wasilewski G. Experimental and numerical investigation of chaotic regions in the triple physical pendulum. *Nonlin. Dyn.* **2007**, 50 (4), 755-766.
15. Dmitriev A.S., Kislov V.Ya. *Stochastic Oscillations in Radiophysics and Electronics*. Nauka: Moscow, **1989**.
16. Awrejcewicz J., Krysko A.V., Papkova I.V., Krysko V.A. Routes to chaos in continuous mechanical systems. Part 3: The Lyapunov exponents, hyper, hyper-hyper and spatial–temporal chaos. *Chaos, Solit. Fract.* **2012**, 45, 721–736
17. Benettin G., Galgani L., Strelcyn J.M. Kolmogorov entropy and numerical experiments. *Phys. Rev. A* **1976,** 14, 2338-2345.
18. Oseledec V.I. A multiplicative ergodic theorem. *Trans. Mosc. Math. Soc*. **1968,** 19, 197-231.
19. Pesin Ya.B. Characteristic Lyapunov exponents and ergodic properties of smooth dynamical systems with invariant measure. *Dokl. Akad. Nauk. SSSR* **1976**, 226, 774-777.
20. Golovko V.A. Neural networks methods of quantifying chaotic process. *Proceedings of VII Conference 'Lectures for Neural Informatics'*. Moscow, **2005**, pp. 43-88 (in Russia).
21. Vallejo J.C., Sanjuan M.A.F. Predictability of orbits in coupled systems through finite-time Lyapunov exponents. *New J. Phys*. **2013**, 15, 113064.
22. Vallejo J.C., Sanjuan M.A.F. *Predictability of Chaotic Dynamics. A Finite-time Lyapunov Exponents Approach*. Springer: Berlin, **2017**.
23. Devaney R.L. *An Introduction to Chaotic Dynamical Systems*. Addison-Wesley: Reading, Mass., **1989**.
24. Banks J., Brooks J., Davis G., Stacey P. On Devaney's definition of chaos. *Am. Math. Month.* **1992,** 99(4), 332-334.
25. Knudsen C. Chaos without periodicity. *Am. Math. Month.* **1994**, 101, 563-565.
26. Gulick D. *Encounters with Chaos*. McGraw-Hill: New York, **1992**.
27. Awrejcewicz J., Krysko V.A., Papkova I.V. Routes to chaos in continuous mechanical systems. Part 1. Mathematical models and solution methods. *Chaos, Sol. Fract*., **2012**, 687-708.
28. Awrejcewicz J., Krylova E.Y., Papkova I.V., Krysko V.A. Wavelet-based analysis of the regular and chaotic dynamics of rectangular flexible plates subjected to shear-harmonic loading. *Shock Vib.* **2012**, 19, 979-994
29. Mackey M.C., Glass L. Oscillation and chaos in physiological control systems. *Science* **1977**, 197, 287–289.
30. Hudson J.L., Mankin J.C. Chaos in the Belousov-Zhabotinskii reaction. *J. Chem. Phys*. **1981**, 74, 6171.
31. Taylor G.I. Stability of a viscous liquid contained between two rotating cylinders. *Phil. Trans. Royal Society A* **1923**, 223(605–615), 289–343.
32. Sato S., Sano M., Sawada Y. Practical methods of measuring the generalized dimension and the largest Lyapunov exponent in high dimensional chaotic systems. *Prog. Theor. Phys*. **1987**, 77, 1-7.
33. Eckmann J.-P., Ruelle D. Ergodic theory of chaos and strange attractors. *Rev. Mod. Phys*. **1985**, 57, 617–656.
34. Sprott J.C. *Chaos and Time Series Analysis*. Oxford University Press: Oxford, **2003**.
35. Sprott J.C. *Elegant Chaos. Algebraically Simple Chaotic Flows*. World Scientific: Singapore, **2010**.